

## An electroactuation system based on nanofluids

Baoxing Xu,<sup>1</sup> Yu Qiao,<sup>2</sup> Yibing Li,<sup>3</sup> Qulan Zhou,<sup>4</sup> and Xi Chen<sup>1,5,6,a)</sup>

<sup>1</sup>Department of Earth & Environmental Engineering, Columbia University, New York, New York 10027, USA

<sup>2</sup>Department of Structural Engineering, University of California, La Jolla, California 92093, USA

<sup>3</sup>Department of Automotive Engineering, Tsinghua University, Beijing 100084, People's Republic of China

<sup>4</sup>State Key Laboratory of Multiphase Flow, Xi'an Jiaotong University, Xi'an 710049, People's Republic of China

<sup>5</sup>SV Laboratory, School of Aerospace, Xi'an Jiaotong University, Xi'an 710049, People's Republic of China

<sup>6</sup>Department of Civil & Environmental Engineering, Hanyang University, Seoul 133-791, Republic of Korea

(Received 16 February 2011; accepted 13 May 2011; published online 3 June 2011)

We propose the conceptual design of an electrically controlled actuation system by adjusting the relative hydrophobicity of a nanoporous material/liquid mixture. When the variation in wettability is amplified by the large surface area, a considerable mechanical work is output. The energy density, power density, and efficiency are explored and their variations with pore size, solid phase, and liquid phase are explored. An infiltration experiment on a nanoporous silica system is performed to qualitatively validate these findings. © 2011 American Institute of Physics.

[doi:10.1063/1.3597367]

At the nanometer-scale surface phenomena become dominant. For example, if a nanoporous solid is soaked in a liquid, the combination of the excess solid-liquid interfacial tension ( $\sim 10\text{--}100\text{ mJ/m}^2$ ) and ultralarge specific surface area ( $\sim 1000\text{ m}^2/\text{g}$ ) can induce an energy change of  $10\text{--}100\text{ J/g}$  or more, making the system very attractive for energy conversion and storage.<sup>1-3</sup>

The effective solid-liquid interfacial tension is a function of electric field,<sup>4,5</sup> which may be employed to control the nanofluidic motion.<sup>6</sup> In this letter, through molecular dynamics (MD) simulations, we propose the basic working mechanism of an electrically controlled actuation system based on nanoporous materials and liquids. In a properly designed system, as the electric intensity varies the effective hydrophobicity would vary so that the system's volume may change and output mechanical work. An electric-induced infiltration experiment is employed to verify the simulation findings.

In the computational model (inset of Fig. 1), a long carbon nanotube (CNT) with hydrophobic inner surface is employed as a model nanopore, with one of its ends inserted into a water reservoir bounded by two rigid planes in the axial direction; the top plane is fixed and the bottom one is moveable (like a piston) so as to adjust the applied pressure. Periodical boundary is imposed in the lateral directions. Water molecules are modeled by the extended simple point charge potential,<sup>7</sup> and the nonbond interaction between water and CNT is described by a Lennard-Jones potential. When other liquid and solid phases are used, the relevant force field parameters are adjusted accordingly.<sup>8</sup> We let the electric field to be parallel to the nanopore wall, which may have more influence on the reduction in surface tension in comparison to a normal field.<sup>9</sup> The magnitude of electric field varies from  $10^{-2}\text{ V/\AA} < E < 0.4\text{ V/\AA}$ , which is typical for ion channels and membranes.<sup>10,11</sup> MD simulation is performed using

LAMMPS with the Canonical ensemble, NVT ensemble at ambient temperature of 300 K.<sup>12</sup>

The model CNT is hydrophobic and thus its inner surface cannot be spontaneously wetted at ambient pressure. By moving the piston upward, the water phase is pressurized and upon a critical infiltration pressure,  $P_{in}$ , the capillary resistance is overcome and infiltration starts. In the example in Fig. 1, the piston moves quasistatically. The relationship between the reservoir pressure and the number of infiltrated water molecules shows that for a (18,18) CNT without electric field, only when the pressure gets beyond  $P_{in}=69\text{ MPa}$ , the water molecules can burst into CNT; the subsequent infiltration curve remains relatively flat due to the smooth wall and low transport resistance inside the CNT.<sup>13</sup> When an external electric field is applied, the effective hydrophobicity is decreased significantly, and  $P_{in}$  reduces almost linearly by more than 70% when  $E$  increases from 0 to  $0.12\text{ V/\AA}$ .

According to the Laplace-Young equation,  $P_{in}=4\gamma/D$ , where  $\gamma$  is the effective interfacial tension and  $D$  is the accessible pore diameter.<sup>2</sup> From classic electrochemistry<sup>14</sup>  $\gamma=\gamma_0-C\phi^2/2$ , where  $\gamma_0$  is the reference wettability in the

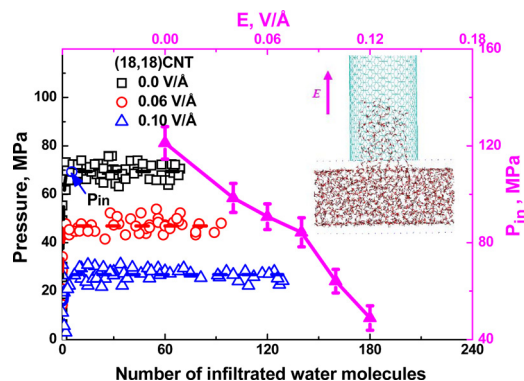


FIG. 1. (Color online) The effect of  $E$  on the infiltration behavior for a (18,18) CNT/water system; the infiltration pressure  $P_{in}$  can be determined accordingly.  $P_{in}$  depends on both  $E$  and pore size.

<sup>a)</sup>Author to whom correspondence should be addressed. Electronic mail: xichen@columbia.edu.

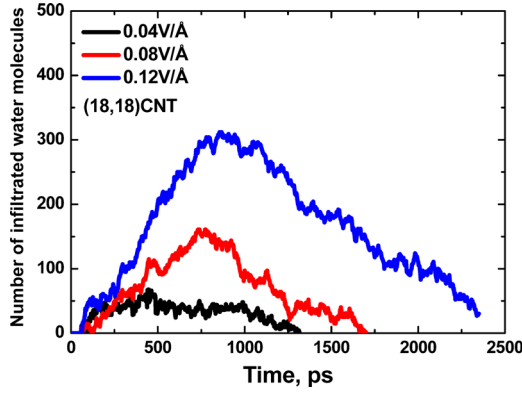


FIG. 2. (Color online) For a (18,18) CNT/water system, when  $P_{app}$  is fixed and upon employment of electric field, the number of infiltrated water molecules varies dramatically with time.

absence of  $E$ ,  $C$  is a positive constant, and  $\phi$  is the applied potential difference. Thus, with the increase in  $E$ ,  $\gamma$  is reduced and the system becomes more wettable. In essence, upon a strong electric field the configuration of the nanoconfined liquid molecules changes, which affects the hydrogen bond, contact angle, as well as the effective surface tension.<sup>15</sup> These factors reduce  $P_{in}$ , and the effect of electric field is coupled with the pore size (confinement) effect.

Figure 1 implies that for a given pore size, there is a one-to-one correspondence between the  $P_{in}$  and  $E$ . Therefore, an electroactuation system can be designed as follows. Let  $P_{in}^0$  and  $P_{in}^E$  to be the critical pressure without and with  $E$ , respectively. An external pressure  $P_{app}$ , whose magnitude is fixed throughout the process and  $P_{in}^0 > P_{app} > P_{in}^E$ , is imposed on the piston. Once the electric field is applied, the system becomes relatively more hydrophilic, and with the water invasion into the nanopore the system volume decreases, and mechanical work is produced. When  $E$  is removed, the system becomes relatively hydrophobic again and the water defiltrates, and part of the stored interfacial tension will be converted to mechanical energy.

We first investigate the performance of a representative actuation system, whose unit cell contains an end-capped (18,18) CNT of length 4.9 nm and initially there are 2312 water molecules in the reservoir. Throughout the simulation, the piston's position is adjusted *in situ* such that the reservoir pressure  $P_{app}$  is kept as a constant just below  $P_{in}^0$ . As expected (Fig. 2), with the application of electric field, the water starts to flow into the CNT. During the operation, the effective work output, which can be evaluated as  $W_{eff} = P_{app} \cdot \Delta V$  with  $\Delta V$  the volume reduction in reservoir, increases almost linearly with time—this implies that the power output  $P$  is almost a constant during actuation. When  $E$  is larger, the water infiltration flow rate,  $q$ , is higher, and thus with higher power. Similar to the classic pipe flow, the flow rate is found to be proportional to the pressure difference,  $q = \xi \cdot (P_{in}^0 - P_{in}^E)$ , and  $\xi$  depends on material and system parameters (and independent of  $E$ ). After  $E$  is removed, the outflow rate is almost the same since that process is driven by the same solid–liquid interfacial tension.

The maximum work ( $W_{max}$ ) that can be output by such a system is reached when the CNT is just filled. Since the infiltrated water molecule configuration depends only slightly on  $E$ , so does  $W_{max}$ . In Fig. 3(a), the down triangle curve gives the relationship between the available energy

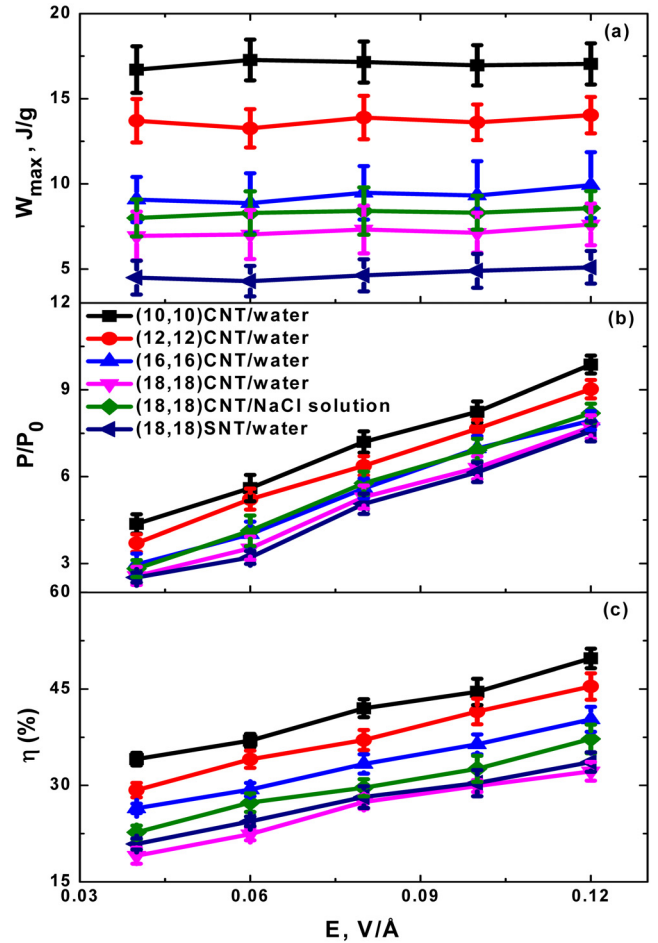


FIG. 3. (Color online) Variation of (a) the maximum work output (energy density),  $W_{max}$  per mass; (b) the normalized output power density,  $P$  (normalized by that of a 1.0 nm<sup>3</sup> water at  $E=0.08$  V/Å); (c) efficiency,  $\eta$ , of the electrically controlled actuation system. The applied electric intensity  $E$ , pore size, pore phase, and liquid phase are varied.

density ( $W_{max}$  per mass, where the mass is that of the entire system) and  $E$  for the current (18,18) CNT/water system with specified dimensions.

The average power density ( $P$  per mass during infiltration) is shown in the down triangle curve in Fig. 3(b), which is a strong function of  $E$ . The system efficiency can be estimated as,  $\eta = W_{eff} / (W_{eff} + W_e) \times 100\%$ , where  $W_e$  is the input required to maintain the static uniform electric field. In Fig. 3(c) the average efficiency of the present system is shown to increase with  $E$  due to the reduced solid–liquid interaction.

The performance of electroactuation depends on characteristics of the system, such as pore phase, pore size, pore length, liquid phase, liquid volume, working temperature, electric field direction, etc. To illustrate, we first study several CNT/water systems with different pore sizes. In these systems the CNT length and reservoir height are fixed, and the ratio between the pore volume and reservoir volume keeps a constant. Corresponding results in Fig. 3 show that, in general, a smaller CNT diameter is more welcome for enhancing the energy density, power density, and efficiency, thanks to the higher surface-to-volume ratio and stronger interfacial action between carbon and water molecules. Nevertheless, it is cautioned that if the CNT is small, the infiltrated water molecules may be constrained in a single-file<sup>8</sup> and that reduces the system performance. When other parameters are

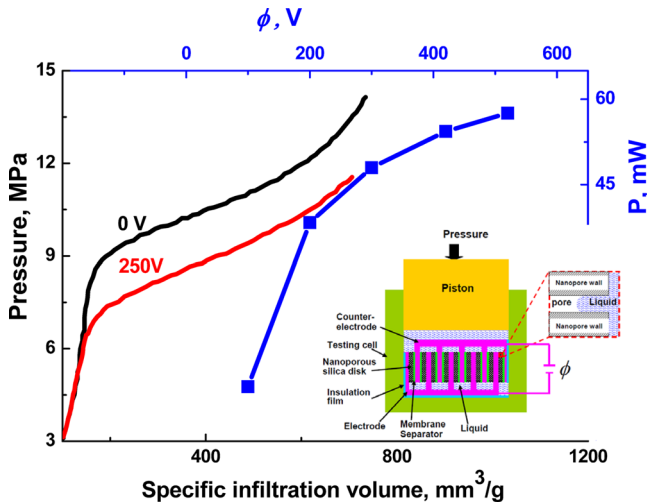


FIG. 4. (Color online) Sorption isotherm experimental curves of the nanoporous silica in KCl-solution with electric field, and variation in output power in the proposed electroactuation system. The inset depicts the experimental setup.

fixed, our study indicates an optimum pore size of about 1 nm.

The CNT can be replaced by other nanochannels, for example, a silica nanotube (SNT) with diameter 24.56 Å that matches with that of CNT (18, 18) and with other conditions fixed. Although the interaction between SNT and water is stronger,<sup>8</sup> SNT is considerably heavier than CNT and thus having lower energy and power densities. When the water phase is replaced by 2.0 mol/l aqueous solution of sodium chloride (NaCl), for the same (18,18) CNT system, the solid-liquid interaction becomes stronger,<sup>8</sup> yet the mass is not significantly increased. Thus for the systems under investigation the energy density, power density, and efficiency are all increased compare with the pure water counterpart.

There are many other factors that can affect actuation. For instance, in all examples above the ratio between the volumes of the pore and reservoir is fixed. If less liquid is used, the energy/power densities and efficiency will improve. The variation in temperature and electric field direction (or pore alignment) will also influence the solid-liquid interfacial tension,<sup>8,16</sup> and a more systematic parametric study will be carried out in future.

To qualitatively validate the computational results, we performed an electrically induced infiltration test on a nanoporous silica crystal. The average  $D=14.6$  nm. Disklike porous silica samples of 16.5 mg were inserted into the adjacent aluminum foils and connected to electrode, Fig. 4. The silica stack is immersed in 10 g of 15% aqueous solution of potassium chloride (KCl) and sealed in a reservoir with proper insulation. A direct current power source with voltage,  $\phi$ , was applied to the system.

The pressure-volume variations in Fig. 4 show similar trends as that in Fig. 1. Due to the nonuniform pore size in the sample, the pressure did not maintain a constant during

the infiltration stage. A significant reduction in  $P_{in}$  is observed when a voltage is applied. The power output of the thus designed electroactuation system is deduced in Fig. 4, which shows that  $P$  increases nonlinearly with  $\phi$ . The energy density is about 4.7 J/g, which, as discussed above, can be significantly improved by using less liquid. The results are qualitatively consistent with simulation, despite of different nanopore structure, solid, and liquid used.

In summary, we propose the concept of an electrically controlled actuation system, by adjusting the effective hydrophobicity of a nanoporous material/liquid system. In the presence of an external electric field the infiltration threshold is reduced and with liquid intrusion the reduction in system volume leads to work output. The power density and efficiency increases with higher electric strength, and for the current system under investigation, the energy density is about 10 J/g and higher. The system performance, such as power density, energy density, and efficiency, also varies with pore size, solid phase, liquid phase, and a few other parameters. The working principles are verified qualitatively by experiment. The study also shed some light on the perspective applications of controlling nanofluidic properties with electric field as well as the design of other electrically controlled nanoscale actuation devices.

The work is supported by NSFC (Grant No. 50928601), World Class University program from Korea NRF (Grant No. R32-2008-000-20042-0), International cooperation project of Tsinghua Univ. (Grant No. 20091081236), Changjiang Scholar Program of China, and NSF (Grant No. CMMI-0643726).

<sup>1</sup>L. Liu, X. Chen, W. Lu, and Y. Qiao, *Phys. Rev. Lett.* **102**, 184501 (2009).

<sup>2</sup>Y. Qiao, L. Liu, and X. Chen, *Nano Lett.* **9**, 984 (2009).

<sup>3</sup>X. Chen, F. B. Surani, X. Kong, V. K. Punyamurtula, and Y. Qiao, *Appl. Phys. Lett.* **89**, 241918 (2006).

<sup>4</sup>C. Y. Won, S. Joseph, and N. R. Alurua, *J. Chem. Phys.* **125**, 114701 (2006).

<sup>5</sup>J. A. Garate, N. J. English, and J. M. D. MacElroy, *J. Chem. Phys.* **131**, 114508 (2009).

<sup>6</sup>M. J. Schertzer, S. I. Gubarenko, R. Ben-Mrad, and P. E. Sullivan, *Langmuir* **26**, 19230 (2010).

<sup>7</sup>H. J. C. Berendsen, J. R. Grigera, and T. P. Straatsma, *J. Phys. Chem.* **91**, 6269 (1987).

<sup>8</sup>J. Zhao, P. J. Culligan, Y. Qiao, Q. Zhou, Y. Li, M. Tak, T. Park, and X. Chen, *J. Phys.: Condens. Matter* **22**, 315301 (2010).

<sup>9</sup>D. Bratko, C. D. Daub, K. Leung, and A. Luzar, *J. Am. Chem. Soc.* **129**, 2504 (2007).

<sup>10</sup>M. L. Berkowitz, D. L. Bostick, and S. Pandit, *Chem. Rev.* **106**, 1527 (2006).

<sup>11</sup>A. Philippsen, W. Im, A. Engel, T. Schirmer, B. Roux, and D. J. Muller, *Biophys. J.* **82**, 1667 (2002).

<sup>12</sup>S. Plimpton, *J. Comput. Phys.* **117**, 1 (1995).

<sup>13</sup>X. Chen, G. Cao, A. Han, V. K. Punyamurtula, L. Liu, P. J. Culligan, T. Kim, and Y. Qiao, *Nano Lett.* **8**, 2988 (2008).

<sup>14</sup>J. O. Bockris, A. K. N. Reddy, and M. Gamboa-Aldeco, *Modern Electrochemistry* (Kluwer Academic, New York, 1998).

<sup>15</sup>C. D. Daub, D. Bratko, K. Leung, and A. Luzar, *J. Phys. Chem. C* **111**, 505 (2007).

<sup>16</sup>L. Liu, J. Zhao, P. J. Culligan, Y. Qiao, and X. Chen, *Langmuir* **25**, 11862 (2009).